nature geoscience

Article

https://doi.org/10.1038/s41561-024-01506-1

Widespread longitudinal snow dunes in Antarctica shaped by sintering

Received: 22 September 2023

Accepted: 15 July 2024

Published online: 23 August 2024

Check for updates

Marine Poizat[1], Ghislain Picard[1], Laurent Arnaud[1], Clément Narteau[2], Charles Amory[1] & Fanny Brun[1]

The surface of Antarctica is continuously shaped by erosion, blowing snow and deposition, resulting in diverse aeolian bedforms akin to those observed in subtropical sand deserts. However, although dunes are universally recognized as a climate and environmental proxy, the properties of snow dunes are not well understood. Here, using satellite images covering most of Antarctica, we report the widespread occurrence (>95% of the area studied) of linear dunes that are between 100 and 1,000 m in length and aligned with the local resultant snow drift direction (61% are longitudinal dunes). On the basis of sand dune theory, we suggest that these snow dunes grow by elongation, often under unidirectional wind regimes. The predominance of the elongating mode indicates a low availability of mobile snow particles. This limited availability prevails at the continental scale due to a subtle balance between snow sintering, which limits erosion, and strong winds, which rapidly remove snowfall. These characteristics result from specific meteorological conditions that distinguish Antarctica from other snow-covered regions, and may shift with future climate changes. We suggest that snow sintering not only influences Antarctic aeolian landform evolution but also regulates the amount of snow sublimated during transport, an uncertain term in the ice-sheet mass balance.

Snow fields in Antarctica exhibit a high diversity of aeolian bedforms, from centimetre-scale ripples[1] to kilometre-scale megadunes[2]. This diversity includes erosional structures, such as sastrugi (as defined in refs. 1,3, which is different from the definition in ref. 4), and depositional features, such as crescent-shaped dunes (~1–20 m wide)[5,6] or linear dunes with a wide range of dimensions (10–1,000 m long, 0.1–1 m high; Fig. 1). These dune shapes are also common in sand deserts[7], in river beds[8] and on other planets and moons[9,10], suggesting similar formation processes despite different fluids and sedimentary environments. Similar to sand dunes, snow dunes are shaped by dynamic interactions that involve topography, wind patterns and particle transport. When snow is transported by wind, dunes develop through erosion/deposition on their upstream/downstream faces as a function of wind acceleration/deceleration. However, contrary to sand, snow particles do not originate only from eroded sediments; snowfalls are a main source. Moreover, snow sublimation contributes to the depletion of snow and the formation of solid bedforms[11]. The understanding of snow dune formation, particularly in Antarctica[3,12–14], is still in its early stages, and the shape, size, orientation and dynamics of dunes have yet to be documented .

Linear snow dunes are difficult to observe from a ground-level perspective as they are extremely flat with a height-to-length ratio typically of <0.001 (for example, in Fig. 1g). Nevertheless, the few scattered observations available suggest that these dunes are very common in Antarctica, and are often, but not always, aligned with the mean wind direction[3,12,15]. They are fundamental landforms because their formation is linked to the accumulation and post-depositional processes[15]. Their mass may constitute an important part of the ice-sheet surface mass balance (SMB), and the average annual snow accumulation height is often lower than the typical dune heights[16], resulting in

[1]IGE, Univ. Grenoble Alpes, CNRS, IRD, Grenoble INP, Grenoble, France. [2]Institut de physique du globe de Paris, Université Paris Cité, CNRS, Paris, France.
e-mail: ghislain.picard@univ-grenoble-alpes.fr

https://doi.org/10.1038/s41561-024-01506-1

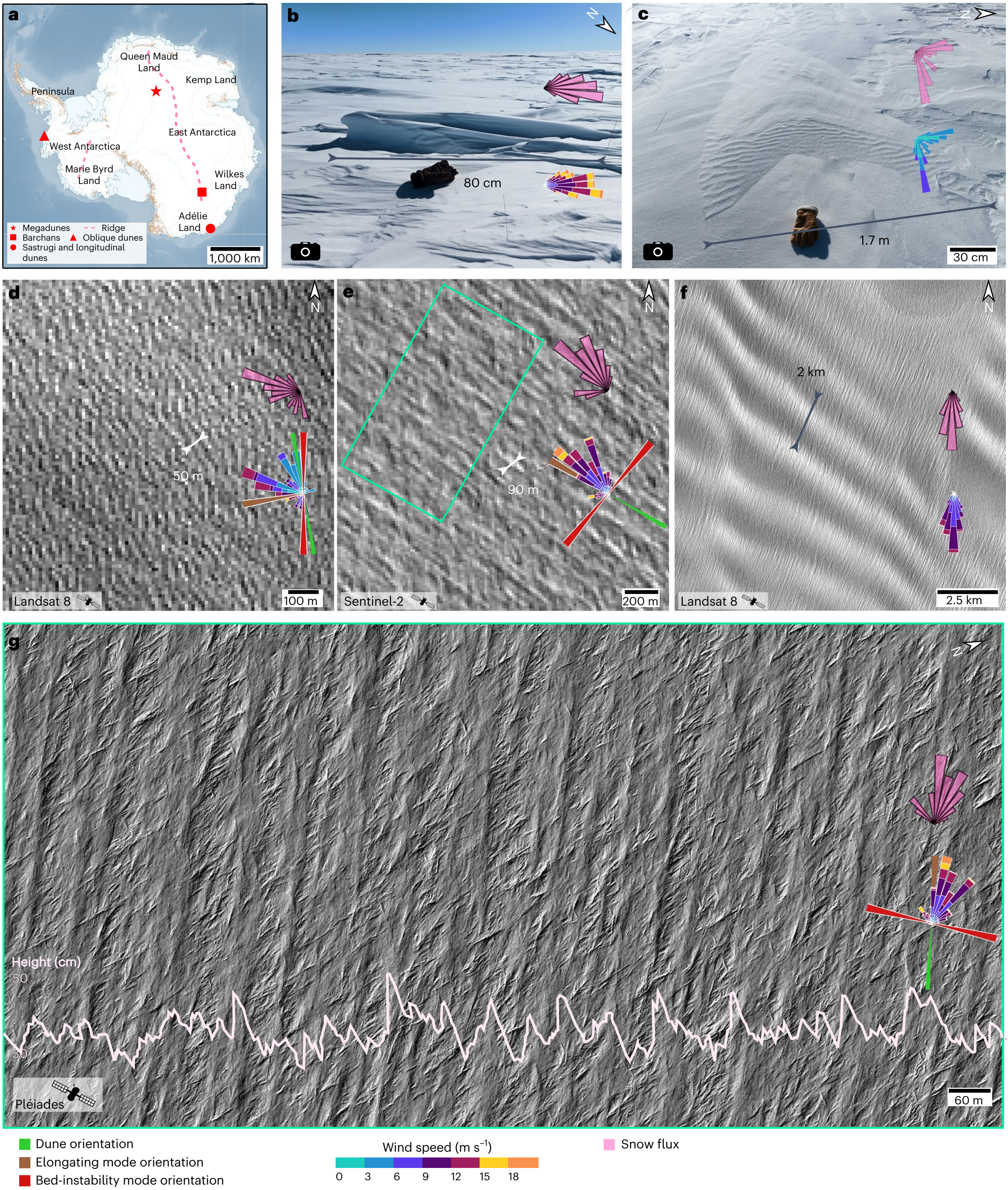

Fig. 1 | Photographs and satellite images of typical snow bedforms found in Antarctica with wind direction. **a**, Map of Antarctica with locations of the bedform images. **b**, Sastrugi (metre-scale erosional structures). **c**, Barchans (metre-scale crescent dunes). **d**, Dunes oblique with respect to the main wind. **e**, Longitudinal dunes. **f**, Megadunes (transverse kilometre-wavelength antidunes). **g**, Expanded image of longitudinal dunes in **e** with the overlaid height profile. The wind roses correspond to the wind regimes since the last snowfall (**d**,**e**,**g**) or the annual wind regime (**f**) from the ERA5 reanalysis. Credit: **g**, Pléiades © CNES (2022), Distribution Airbus DS.

the persistence of these dunes over months to years. Furthermore, dunes contribute to the surface roughness, with implications for the aerodynamic drag of the atmosphere[17]. They also enhance the snowpack heterogeneity and disturb the typical layered structure found in low-wind regions. This heterogeneity reduces the accuracy of SMB measurements[18], SMB modelling[19], remote sensing measurements[20,21] and ice core interpretation[22,23]. Consequently, the study of snow dunes is related to some of the main research questions on the ice sheets.

Wind regimes and the availability of mobile particles are known to govern the shape of aeolian sand dunes in subtropical deserts[24]. They also control dune alignment with respect to the resultant drift direction (RDD; the mean sediment flux direction). Indeed, two dune growth mechanisms have been identified, such that the same wind regime can lead to two different dune orientations depending on the sediment availability for transport[25,26]. Under abundant availability of particles, dune patterns grow in height. In this case, according to the dune instability theory[27], dunes align in the direction of maximum growth rate (bed-instability mode). Considering the divergence angle ζ between the dune alignment and the RDD, the bed-instability mode can lead to transverse orientation ($\zeta > 75°$) or, especially when the wind is multidirectional, oblique ($15° < \zeta < 75°$) and longitudinal ($15° < \zeta$) orientations[26]. Under limited availability of mobile particles, dunes can also elongate in the direction of the resultant sand flux at their crest by depositing at their tips the particles transported along their flanks (elongating mode). This elongating mode can produce only oblique or longitudinal dunes[26]. Considering only transport processes, elongation should not occur under unidirectional wind regimes, for which only trains of barchan dunes should be observed[25]. However, elongating dunes produced by a single prevailing wind have been reported in many deserts on Earth, as well as on Mars and Titan, when cohesive processes are involved (for example, vegetation or electrostatic forces)[28–30].

Here we investigate the distribution and orientation of hectometre linear dunes at the scale of Antarctica to identify the dominant dune growth mechanisms and evaluate the key role of snow sintering, which is a chief source of cohesive force development for snow. Thus, we decipher how dunes are formed in Antarctica, and shed light on the availability of mobile snow over the entire ice sheet.

Ubiquity of longitudinal dunes

The spatial distribution and orientation of the linear snow dunes are retrieved from satellite imagery. All 33,000 available satellite optical images acquired in November and December from 2018 to 2021, which covers ~7.5×10^6 km^2 (~60% of the continent, excluding observation gaps, crevasses and so on), are processed (Methods). With a resolution of 10–15 m, only dunes longer than 20 m are captured, excluding smaller features such as barchans from our analysis. We retrieve dune orientations using two-dimensional (2D) spatial autocorrelation on every subimage (2.56 × 2.56 km and 3.84 × 3.84 km for Sentinel-2 and Landsat 8, respectively (Methods)). Objects that are larger than a kilometre, especially megadunes, are therefore excluded[13,14]. Figure 2 shows the mean dune orientation aggregated over 4 years (the full-resolution image is shown in Extended Data Fig. 1). The interannual variability in dune occurrence and orientation is small (Supplementary Figs. 1 and 2), so our analysis excludes the dynamics and instead focuses on the general and recurrent mean patterns.

The results highlight that linear dunes are widespread in Antarctica, covering over 95% of the studied surface (Fig. 2). Their ubiquity suggests that favourable formation conditions exist all over the continent, despite a wide range of wind regimes[31] and snowfall amounts. They are even present in areas of low accumulation or erosion (Supplementary Fig. 3). This confirms the relative independence of these linear dunes with respect to other smaller and bigger snow bedforms. The remaining 5% without detected dunes are mainly located over the Antarctic Plateau above 3,000 m above sea level (masl), where the wind is generally weak (mean wind speed 6.2 m s^{-1}) and multidirectional (Fig. 2b), and snowfalls are limited (mean of 50 kg m^{-2} y^{-1}).

The map of dune orientations features a few wide and uniform spatial domains. In East Antarctica, these domains extend to lengths of >1,000 km, whereas West Antarctica presents smaller-scale variations (~200 km). The East Antarctica divide (also known as the ice ridge; long pink dashed line Fig. 1a) separates the dune field orientation into two areas. The outer region, located between the coasts and the divide (mainly with blue colours in Fig. 2a, latitude < 76° S), exhibits orientations of around 120° (with respect to the north, positive eastwards) whereas the inner region (chiefly brown and yellow colours) shows orientations of around 25°. Similarly in West Antarctica, the divide (short pink dashed line Fig. 1a) delineates the outer regions with orientations of around 114° and inland regions with orientations of around 45° (Fig. 2). These patterns are stable over years, even though the lifetime of individual dunes ranges from several months to more than a year (Supplementary Figs. 1 and 4).

The wind regimes for 2018–2021 (Fig. 2b), extracted from the ERA5 reanalysis, show a clear general pattern. In East Antarctica, the divide distinguishes itself with multidirectional wind regimes (spread out roses) and low wind speeds (Fig. 2b). There, the mean directional wind constancy—which tends to unity for a unidirectional wind regime and zero for a uniformly random wind direction—is about 0.70 (Supplementary Fig. 6), well below the continent median of 0.89. In the outer regions, cold air accelerates by gravity down steep slopes from the flat inland plateau, creating strong and unidirectional katabatic winds along the coasts, with a mean directional constancy of 0.83 and a mean wind speed of 8.2 m s^{-1} (Fig. 2b)[31]. In West Antarctica, the situation is more spatially variable, as noted for dune orientations. In Marie Byrd Land, the mean constancy is 0.68, whereas it is as low as 0.45 in the Antarctic Peninsula.

The dune orientation with respect to the RDD is derived from both maps in Fig. 2 (Methods). The results (Supplementary Fig. 7) show that dunes are mostly longitudinal (61%) (Methods). Oblique dunes account for 36% in the detected dune area, and transverse dunes account for only 3% (Supplementary Fig. 8). The longitudinal dunes clearly dominate over Antarctica, which suggests that a particular and similar mechanism is involved in their formation. The predominance of longitudinal dunes is more marked in East Antarctica (68%) than in West Antarctica (40%). Eighty-five per cent of the longitudinal dune areas correspond to regions with a wind directional constancy larger than 0.80 (Supplementary Fig. 9), that is, regions where the wind is highly unidirectional, whereas for 85% of the oblique dune area, the directional constancy is only larger than 0.64. Oblique or transverse dunes are mainly found over the East Antarctic divide and Marie Byrd Land.

Dune formation modes

The formation of sand dunes can be explained via two different modes (elongating and bed-instability modes)[26,32]. These modes result in different dune orientations, even under the same wind regime. To evaluate the potential of this theory in explaining the orientation of linear snow dunes, we calculated the snow flux from the wind regime for the 2018–2021 period for each pixel (0.25° × 0.25° resolution) and computed the theoretical orientation (detailed equations in Methods) for each mode (Supplementary Fig. 10). Then, we selected the mode with the closest agreement to the observed dune orientation, provided that the agreement is better than 15°. The resulting map of mode dominance (Fig. 3) highlights that for 63% of the studied area, dune orientation can be explained using either mode. The elongating mode is by far predominant (97% of the explained area). As noted for the wind regimes and dune orientations, the situation is more uniform in East Antarctica with 70% of explained orientation compared with only 42% in West Antarctica. In both regions, the elongating mode corresponds mainly to longitudinal dune areas (89%; Supplementary Table 1). By contrast, the bed-instability mode is rare, at around 2% of the studied area, and

 https://doi.org/10.1038/s41561-024-01506-1

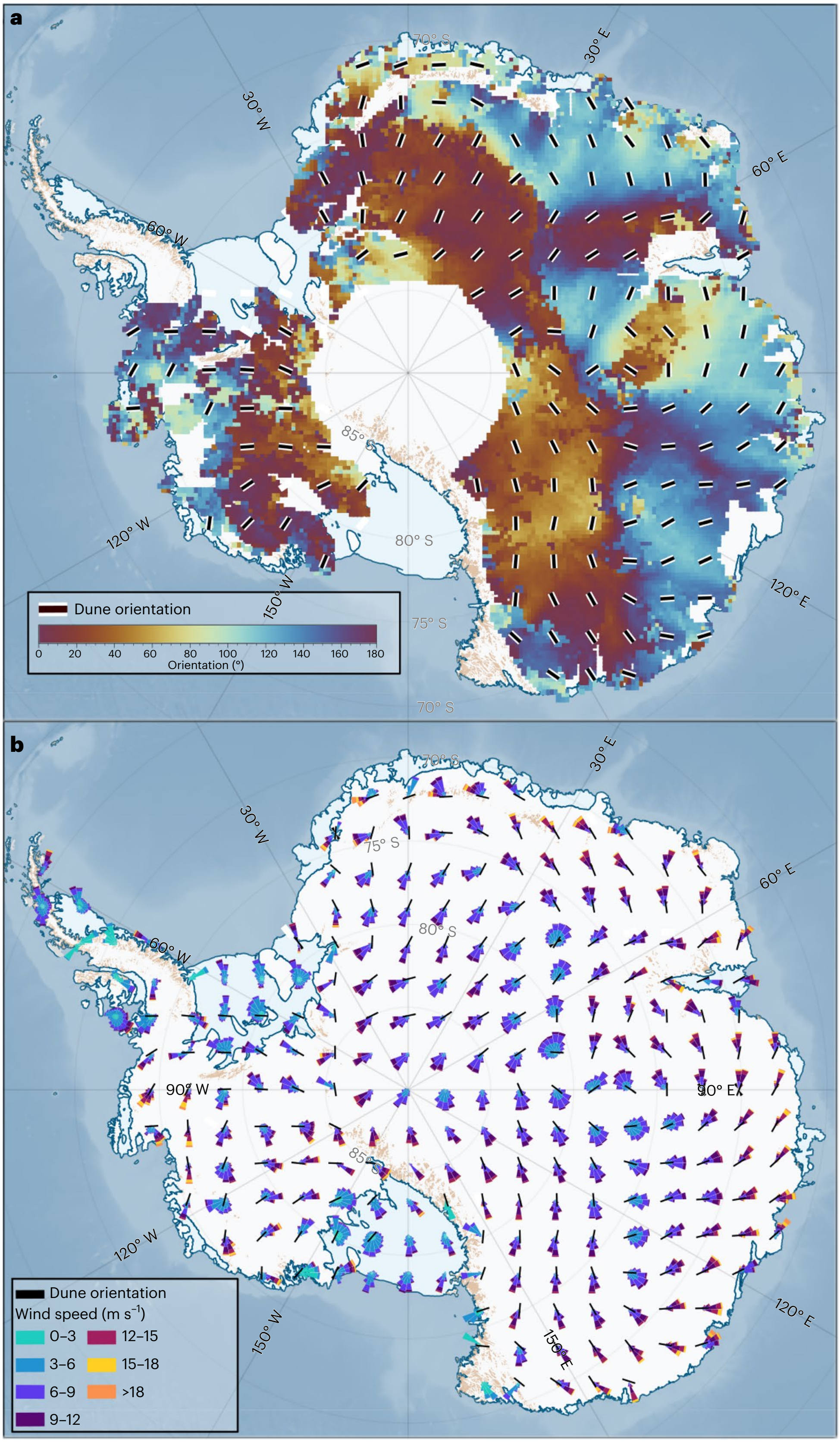

Fig. 2 | Dune orientations and wind direction. a, Map of the dune orientation (0° at the geographical north, +90° eastwards; the colour scale is cyclic from 0 to 180°, the direction of the dune orientation is not identified). Dune orientation over a 25 × 25 km area retrieved from satellite imagery between November and December from 2018 to 2021 (Methods). **b**, Wind roses in Antarctica calculated via ERA5 meteorological reanalysis from 2018 to 2021, and observed dune orientation (spaced every 250 km).

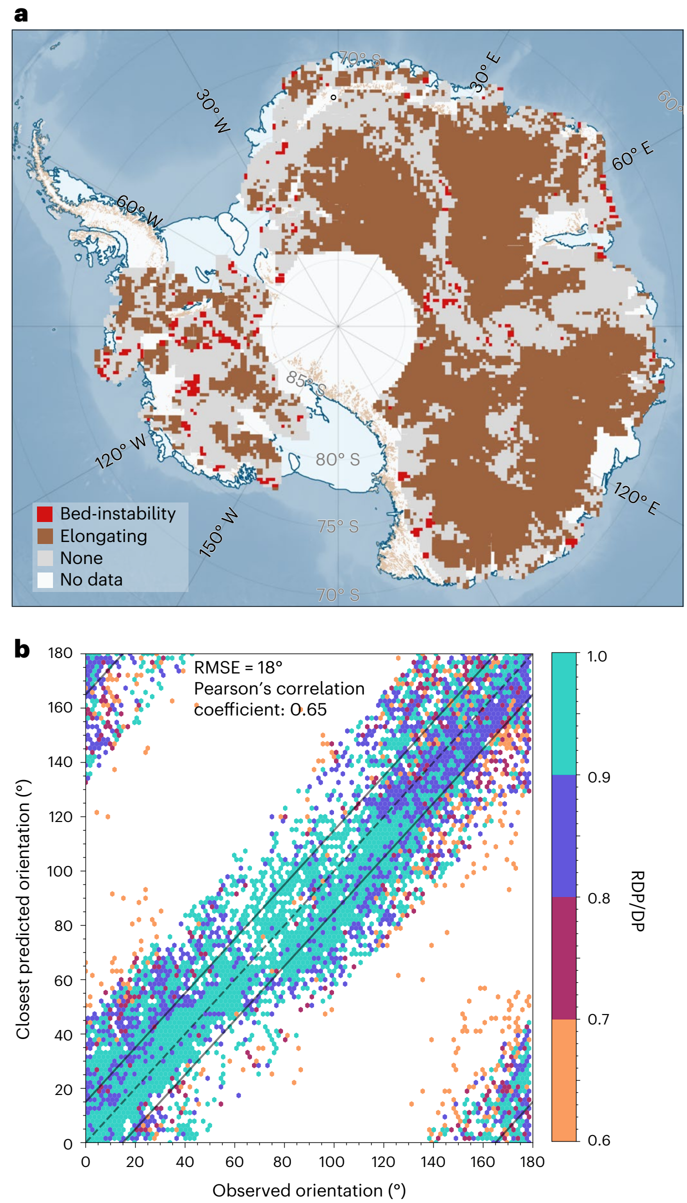

Fig. 3 | Spatial distribution of the mode and comparison with the observations. a, Map of the dominant dune formation mode. The dominant mode is obtained by comparing the observed dune orientations with the calculated orientations of the elongating and bed-instability modes. The wind data are derived from ERA5 reanalysis with a resolution of 0.25° × 0.25°. **b**, Orientation of the dominant mode as a function of the observed dune orientation. The 1:1 dashed dark grey line and the 1:1 ± 15° solid dark grey lines represent perfect agreement between the observed and predicted dune orientations. The ratio of the resultant drift potential to the drift potential (that is, RDP/DP) characterizes the directional variability of the snow flux (flux constancy). When $\frac{\mathrm{RDP}}{\mathrm{DP}} \to 1$ the flux tends to be unidirectional, whereas when $\frac{\mathrm{RDP}}{\mathrm{DP}} \to 0$ it is multidirectional. RMSE, root mean squared error.

most often corresponds to transverse (54%) and oblique (43%) dunes (Supplementary Table 1).

The observed orientations cannot be explained in 37% of the studied area. This is the case around the East Antarctic divide, in Marie Byrd Land (62% of unexplained regions) and on the coast of Adélie Land and Kemp Land. These areas mainly correspond to oblique dunes (77%) rather than longitudinal (18%) or transverse dunes (5%). These regions are usually where two different dune orientations have been detected (30%) or where the wind regime is multidirectional (50% of these regions have a wind directional constancy lower than 0.85; Fig. 3b). The combination of multidirectional wind regimes and multiple dune orientations makes these areas more complex compared with others.

Dunes as indicators of the snow availability

We have established that longitudinal dunes are predominant in Antarctica (61% of the studied area). This predominance is similar in the Earth's sand deserts (with an average of 66%; ref. 33) and is even more pronounced on Titan (95%; ref. 34). In addition, we found that the elongating mode is the main formation mode of the longitudinal dunes in Antarctica. Courrech du Pont et al.[26] established that sediment availability was the key determinant of the mode dominance. The bed-instability mode requires abundant sediment, which, in the case of snow, can be provided not only by surface erosion but also by snowfall. Our result demonstrating the predominance of the elongating mode clearly indicates that snow availability is limited almost everywhere in Antarctica.

At the scale of the continent, snow availability is controlled by the amount of snowfall, surface sublimation and by snow cohesion. Snowfall generally decreases inland, resulting in an extremely dry interior (with a mean of 50 kg m^{-2} y^{-1} above 3,000 masl), which is therefore logically dominated by the elongating mode. By contrast, the coastal regions receive abundant snowfall (~800 kg m^{-2} y^{-1}), but surprisingly the bed-instability mode is infrequent there. This apparent contradiction could be resolved by accounting for the overall increase in wind speed from the interior towards the coasts. Although wind is necessary to form dunes, winds that are too strong may rapidly remove available sediment and enhance surface sublimation and erosion, hence promoting the elongating mode[35]. This suggests that regions with strong winds and large snowfall may only be suitable for the bed-instability mode for short periods during and just after snowfalls, whereas the elongating mode is dominant most of the time. We therefore conclude that the predominance of the elongating mode in the coastal regions is indicative of important mobile snow removal from the surface. This can be due to surface sublimation and erosion. In the latter case, it may indicate a substantial export of snow out of the ice sheet from upstream areas up to hundreds of kilometres[36,37]. Alternatively, it could suggest considerable snow cohesion in these regions.

Sublimation depends strongly on the snow and air temperatures, due to the non-linearity of the relation (Clausius–Clapeyron, for example), and the air relative humidity[11]. It can occur either at the surface or more efficiently during transport[38,39]. On average over the continent, surface sublimation removes 7.5% of the precipitation and blowing snow sublimation removes 3.3% (ref. 40). Blowing snow sublimation exhibits strong spatial variations, and is more important over the coasts where the snow transport is more intense[40,41]. Therefore, erosion and sublimation cannot explain the scarcity of mobile snow particles alone.

Another factor that controls availability is the cohesion between snow particles. Unlike sand, snow cohesion usually increases over time after deposition because ice bonds between crystals are progressively formed by sintering[42,43]. As a result of this cohesion, the minimum wind speed required to erode snow generally increases over time, and the flux of blowing snow progressively decreases after a snowfall[44,45]. In addition, the sintering rate increases exponentially with temperature, and the cohesion is promoted by the repeated particle rebounds during blowing snow events[43,44]. This is why, in the cold and windless interior of the continent, snow may remain mobile for many months[16]. However, in coastal regions, sintering and sublimation are promoted by high temperature (that is, temperatures greater than −20 °C), and the availability of snow can decrease in only a few days[6,46]. Results from a numerical model initially developed for sand dunes[47] showed that cohesion can stop dune motion[48], suggesting that some dunes may not adapt to successive wind regimes. For example, in a sequence of satellite images over 15 days (Supplementary Fig. 5), we highlighted the re-orientation from the long-term average direction to the orientation that was predicted with the wind during the storm only, which are generally different (Supplementary Fig. 11), with no further adaptation (Supplementary Fig. 4). This is possible because the amount of snowfall for this event was significant, that is, 10 kg m^{-2}, which is sufficient, for instance, to form 500-m-long and 40-cm-high linear dunes, as observed in Fig. 1. Therefore, the interpretation of dune orientations may require the wind regimes during the last significant snowfall to be considered (Supplementary Fig. 12b, faded red). This may explain why two different dune directions can coexist in some regions in Antarctica. These examples suggest that the dune formation and evolution dynamics deserve further work to understand dunes beyond the overall long-term patterns depicted in this study.

Implications for the climatology of Antarctica

Our study shows the ubiquitous presence of snow dunes in Antarctica. Moreover, dune orientations can be successfully linked to the wind regime through sand dune theory, thus demonstrating the similarity of the physical principles among different geomaterials and environments. These results will greatly facilitate the next steps towards an improved understanding and quantitative modelling of snow dune formation. For instance, the other characteristics of the linear dunes (size, migration speed and lifetime) can be investigated in light of sand and river bedform knowledge. Our finding of widespread conditions for low snow availability has large implications for an understanding of the snow processes of Antarctica's climatology. In the coastal regions, this provides new insights about the fate of snowfall, with two different pathways. Either the cohesion at the surface increases rapidly, letting new snow settle, or a large part of the snowfall is rapidly removed by wind, partially sublimated and potentially exported out of the ice sheet to the ocean. The contribution of each pathway to the SMB of the ice sheet is radically different and currently a debated question. Rapid snow settling leads to surface accumulation, whereas sublimation during transport or export to the ocean leads to surface ablation. Recent modelling studies have estimated that export to the ocean is insignificant[39,40,49], which is consistent with our results that suggest important sintering. However, regarding blowing snow sublimation, the few model estimates that are currently available in the literature show a large disparity in sublimation rates of up to 290% (refs. 40,41,50). This disparity originates from the modelling difficulties of blowing snow estimates, which are poorly constrained, despite their importance to better constrain the SMB. Owing to the omnipresence of the elongating mode, we argue that an important part of the precipitation contributes to the dune formation (for example, from the Pléiades satellite image, the dune mass represents roughly 15–40% of the annual precipitation at location D47), and that snow sinters rapidly, making it unavailable for transport. This estimation of the dune mass, along with the stability of the patterns (Supplementary Fig. 1), the persistence of dunes during summer (Supplementary Fig. 4), the absence of superimposed bed-instability dunes (Fig. 1) and the predominance of the elongating mode (Fig. 3), all together indicate the importance of sintering. Understanding sintering is necessary not only to gain insight into the stability and formation of dunes but also into snow transport, especially into the threshold wind speed, and therefore improves estimations of the actual ice-sheet SMB. Furthermore, as the contribution of these pathways depends on a subtle balance between the precipitation amount, wind strength and temperature, changes in dune types are to be expected in a future warmer and windier climate.

Online content

Any methods, additional references, Nature Portfolio reporting summaries, source data, extended data, supplementary information, acknowledgements, peer review information; details of author contributions and competing interests; and statements of data and code availability are available at https://doi.org/10.1038/s41561-024-01506-1.

References

1. Doumani, G. A. Surface structures in snow. In *Proc. Conference on the Physics of Snow and Ice* Vol. 1 (ed. Ôura, H.) 1119–1136 (Institute of Low Temperature Science, 1967).
2. Frezzotti, M., Gandolfi, S., Marca, F. L. & Urbini, S. Snow dunes and glazed surfaces in Antarctica: new field and remote-sensing data. *Ann. Glaciol.* **34**, 81–88 (2002).
3. Watanabe, O. Distribution of surface features of snow cover in Mizuho Plateau. *Mem. Natl Inst. Polar Res. Spec. Issue* **7**, 44–62 (1978).
4. Mather, K. B. Further observations on sastrugi, snow dunes and the pattern of surface winds in Antarctica. *Polar Rec.* **11**, 158–171 (1962).
5. Kobayashi, S. & Ishida, T. Interaction between wind and snow surface. *Boundary Layer Meteorol.* **16**, 35–47 (1979).
6. Filhol, S. & Sturm, M. Snow bedforms: a review, new data, and a formation model. *J. Geophys. Res. Earth Surf.* **120**, 1645–1669 (2015).
7. Lancaster, N. *Geomorphology of Desert Dunes* (Cambridge Univ. Press, 2023).
8. Best, J. The fluid dynamics of river dunes: a review and some future research directions. *J. Geophys. Res. Earth Surf.* https://doi.org/10.1029/2004JF000218 (2005).
9. Rubanenko, L., Lapôtre, M. G. A., Ewing, R. C., Fenton, L. K. & Gunn, A. A distinct ripple-formation regime on Mars revealed by the morphometrics of barchan dunes. *Nat. Commun.* **13**, 7156 (2022).
10. Telfer, M. W. et al. Dunes on Pluto. *Science* **360**, 992–997 (2018).
11. Bordiec, M. et al. Sublimation waves: geomorphic markers of interactions between icy planetary surfaces and winds. *Earth Sci. Rev.* **211**, 103350 (2020).
12. Okuhira, F. et al. A study of formation of a surface snow layer. *Mem. Natl Inst. Polar Res. Spec. issue* **7**, 140–153 (1978).
13. Dadic, R., Mott, R., Horgan, H. J. & Lehning, M. Observations, theory, and modeling of the differential accumulation of Antarctic megadunes. *J. Geophys. Res. Earth Surf.* **118**, 2343–2353 (2013).
14. Traversa, G., Fugazza, D. & Frezzotti, M. Megadunes in Antarctica: migration and characterization from remote and in situ observations. *Cryosphere* **17**, 427–444 (2023).
15. Goodwin, I. D. Snow accumulation and surface topography in the katabatic zone of eastern Wilkes Land, Antarctica. *Antarct. Sci.* **2**, 235–242 (1990).
16. Picard, G., Arnaud, L., Caneill, R., Lefebvre, E. & Lamare, M. Observation of the process of snow accumulation on the Antarctic Plateau by time lapse laser scanning. *Cryosphere* **13**, 1983–1999 (2019).
17. Vignon, E. et al. Stable boundary-layer regimes at Dome C, Antarctica: observation and analysis. *Q. J. R. Meteorol. Soc.* **143**, 1241–1253 (2017).
18. Weller, G. The heat and mass balance of snow dunes on the central Antarctic plateau. *J. Glaciol.* **8**, 277–284 (1969).
19. Amory, C. et al. Seasonal variations in drag coefficient over a sastrugi-covered snowfield in coastal East Antarctica. *Boundary Layer Meteorol.* **164**, 107–133 (2017).
20. Corbett, J. & Su, W. Accounting for the effects of sastrugi in the CERES clear-sky Antarctic shortwave angular distribution models. *Atmos. Meas. Tech.* **8**, 3163–3175 (2015).
21. Fraser, A. D. et al. Drivers of ASCAT C band backscatter variability in the dry snow zone of Antarctica. *J. Glaciol.* **62**, 170–184 (2016).
22. Ekaykin, A. et al. Non-climatic signal in ice core records: lessons from Antarctic megadunes. *Cryosphere* **10**, 1217–1227 (2016).
23. Zuhr, A. M., Münch, T., Steen-Larsen, H. C., Hörhold, M. & Laepple, T. Local-scale deposition of surface snow on the Greenland ice sheet. *Cryosphere* **15**, 4873–4900 (2021).

24. Wasson, R. J. & Hyde, R. Factors determining desert dune type. *Nature* **304**, 337–339 (1983).
25. Gao, X. Phase diagrams of dune shape and orientation depending on sand availability. *Sci. Rep.* **5**, 14677 (2015).
26. Courrech du Pont, S., Narteau, C. & Gao, X. Two modes for dune orientation. *Geology* **42**, 743–746 (2014).
27. Lü, P. et al. Direct validation of dune instability theory. *Proc. Natl Acad. Sci. USA* **118**, e2024105118 (2021).
28. Rubin, D. M. & Hesp, P. A. Multiple origins of linear dunes on Earth and Titan. *Nat. Geosci.* **2**, 653–658 (2009).
29. Herrmann, H. J., Durán, O., Parteli, E. J. R. & Schatz, V. Vegetation and induration as sand dunes stabilizators. *J. Coast. Res.* **24**, 1357–1368 (2008).
30. Méndez Harper, J. S. et al. Electrification of sand on Titan and its influence on sediment transport. *Nat. Geosci.* **10**, 260–265 (2017).
31. King, J. C. & Turner, J. *Antarctic Meteorology and Climatology* (Cambridge Univ. Press, 1997).
32. Lucas, A. et al. Sediment flux from the morphodynamics of elongating linear dunes. *Geology* **43**, 1027–1030 (2015).
33. Lancaster, N. Linear dunes. *Prog. Phys. Geogr. Earth Environ.* **6**, 475–504 (1982).
34. Radebaugh, J. et al. Dunes on Titan observed by Cassini radar. *Icarus* **194**, 690–703 (2008).
35. Amory, C. Drifting-snow statistics from multiple-year autonomous measurements in Adélie Land, East Antarctica. *Cryosphere* **14**, 1713–1725 (2020).
36. Palm, S. P., Yang, Y., Spinhirne, J. D. & Marshak, A. Satellite remote sensing of blowing snow properties over Antarctica. *J. Geophys. Res. Atmos.* https://doi.org/10.1029/2011JD015828 (2011).
37. Scarchilli, C. et al. Extraordinary blowing snow transport events in East Antarctica. *Clim. Dyn.* **34**, 1195–1206 (2010).
38. Bintanja, R. Snowdrift sublimation in a katabatic wind region of the Antarctic ice sheet. *J. Appl. Meteorol. Climatol.* **40**, 1952–1966 (2001).
39. Agosta, C. et al. Estimation of the Antarctic surface mass balance using the regional climate model MAR (1979–2015) and identification of dominant processes. *Cryosphere* **13**, 281–296 (2019).
40. Gerber, F., Sharma, V. & Lehning, M. CRYOWRF—model evaluation and the effect of blowing snow on the Antarctic surface mass balance. *J. Geophys. Res. Atmos.* **128**, e2022JD037744 (2023).
41. Palm, S. P., Kayetha, V., Yang, Y. & Pauly, R. Blowing snow sublimation and transport over Antarctica from 11 years of CALIPSO observations. *Cryosphere* **11**, 2555–2569 (2017).
42. Colbeck, S. C. *A Review of Sintering in Seasonal Snow* CRREL Report 97-10 (US Army Cold Regions Research and Engineering Laboratory, 1997).
43. Blackford, J. R. Sintering and microstructure of ice: a review. *J. Phys. D Appl. Phys.* **40**, R355–R385 (2007).
44. Comola, F., Gaume, J., Kok, J. F. & Lehning, M. Cohesion-induced enhancement of aeolian saltation. *Geophys. Res. Lett.* **46**, 5566–5574 (2019).
45. Melo, D. B., Sharma, V., Comola, F., Sigmund, A. & Lehning, M. Modeling snow saltation: the effect of grain size and interparticle cohesion. *J. Geophys. Res. Atmos.* **127**, e2021JD035260 (2022).
46. Kaempfer, T. U. & Schneebeli, M. Observation of isothermal metamorphism of new snow and interpretation as a sintering process. *J. Geophys. Res. Atmos.* https://doi.org/10.1029/2007JD009047 (2007).
47. Narteau, C., Zhang, D., Rozier, O. & Claudin, P. Setting the length and time scales of a cellular automaton dune model from the analysis of superimposed bed forms. *J. Geophys. Res. Earth Surf.* https://doi.org/10.1029/2008JF001127 (2009).
48. Sharma, V., Braud, L. & Lehning, M. Understanding snow bedform formation by adding sintering to a cellular automata model. *Cryosphere* **13**, 3239–3260 (2019).
49. Van Wessem, J. M. et al. Modelling the climate and surface mass balance of polar ice sheets using RACMO2 – part 2: Antarctica (1979–2016). *Cryosphere* **12**, 1479–1498 (2018).
50. Gadde, S. & van de Berg, W. J. Contribution of blowing snow sublimation to the surface mass balance of Antarctica. Preprint at *EGUsphere* https://doi.org/10.5194/egusphere-2024-116 (2024).

https://doi.org/10.1038/s41561-024-01506-1

Methods

Dune orientation retrieval from satellite imagery

We retrieve dune orientation data from Landsat 8 and Sentinel-2 images, which have, respectively, a resolution of 15 m and 10 m (refs. 51,52). Owing to their Sun-synchronous orbits, Landsat 8 and Sentinel-2 images are only available north of around 83° S, leading to a surface of ~2×10^6 km^2 that is not covered around the South Pole. We selected the near-infrared channel of Sentinel-2 (NIR channel, band 8) to maximize image contrast, and the highest spatially resolved panchromatic band of Landsat 8 (PAN channel, band 8), and use 2D spatial autocorrelation to estimate the orientation, a technique used successfully for sand dune detection and detailed in ref. 25. The method is applied over every $N = 256 \times 256$ pixel subimage, which corresponds to 3.84 × 3.84 km for Landsat 8 and 2.56 × 2.56 km for Sentinel-2. We exclude the mountains and probable crevasse areas (that is, areas with a flow speed of greater than 40 m y^{-1} as extracted from the NASA MEaSUREs ice velocity map[53,54]) as they disturb detection of the dune orientation. These crevassed areas are mainly located over the Peninsula and the coasts. Notably, most blue-ice areas (retrieved using the mapping from ref. 55, directly available in the Quantarctica package[56]) are excluded due to the presence of crevasses. The following method used for retrieval of the dune orientation from satellite images is summarized in Supplementary Fig. 14.

Step 1. Clouds are removed. Clouds are detected using a threshold on the reflectance in the blue and short-wave infrared bands[57]. If clouds cover more than 10% of a subimage, the subimage is completely discarded; otherwise, nearest-neighbour interpolation is performed to fill the gaps caused by the clouds.

Step 2. On every subimage of size $N \times N$, the 2D autocorrelation at the position (x,y) in the subimage is calculated using the Wiener–Khintchine theorem:

$$\mathrm{AC}(x,y) = F^{-1}\left(|F(v(x,y))|^2\right), \tag{1}$$

where $\mathrm{AC}(x,y)$ is the autocorrelation function, $v(i,j)$ is the image intensity for pixel (i,j) and F is the Fourier transform.

Step 3. The dune orientation α is obtained by searching the maximum of

$$f\left(\alpha + \frac{\Delta\alpha}{2}\right) = \int_0^R \int_\alpha^{\alpha+\Delta\alpha} \mathrm{AC}(r,\theta) r \, \mathrm{d}r \, \mathrm{d}\theta$$

where r and θ are the polar coordinates, respectively the radius and the angle (Supplementary Fig. 15). This double integral is calculated for angles between 0 and 360°, with $\Delta\alpha = 3°$ for three different radii of $R = 16$, 32 and 64 pixels. If a secondary maximum exists and is larger than the 95% quantile of the integral, it is considered to be the second orientation. It is worth noting that the dune direction is not identified, that is, the dune orientation is between 0 and 180°.

Step 4. The orientations from all of the subimages at all dates during the period (November and December for 2018, 2019, 2020 and 2021) are projected on to a regular stereographic grid (ESPG:3031) spaced by 2.56 km. On each grid point, the orientations are combined by taking the maximum of the probability density function estimated using the circular kernel density estimation[58]. The redundancy of information (typically four subimages for a given location) enable us to reduce the impact of artefacts (undetected clouds, stripes, banding and so on) and the uncertainties in the orientation estimates. Finally, we obtain the final dune orientation grid. The orientation accuracy is around 5°.

Step 5. Wind data are retrieved from the ERA5 reanalysis hourly data on single levels from 1940 to the present[59], which have been evaluated over Antarctica[60–62] and show a similar performance to the other reanalyses with an underestimation of strong winds, especially in the coastal regions. For comparison with the ERA5 reanalysis wind data that are available at 0.25° × 0.25° resolution, we aggregate the orientations to this roughly tenfold coarser resolution using the circular kernel density estimation as in Step 4. The resulting orientation is then compared with the consequent RDD ω value for 2018–2021, which is calculated with $\tan\omega = \frac{\Sigma_{i=2018}^{2021} u_i}{\Sigma_{i=2018}^{2021} v_i}$, where u_i is the eastward component of the flux, v_i is the northward component of the flux and i is the index over time. The resultant drift potential (RDP) is the norm of the mean snow flux vector. The drift potential (DP) is the mean of the norms of the snow flux vectors, that is, $\Sigma_{t=2018}^{2021} \| \overrightarrow{\mathrm{flux}(t)} \|$ over $\| \Sigma_{t=2018}^{2021} \overrightarrow{\mathrm{flux}(t)} \|$. The ratio RDP/DP gives the constancy of the flux. The value tends to unity when the flux is unidirectional and to zero when the flux is multidirectional.

Dune orientation model

Courrech du Pont et al.[26] identified two modes of formation for the sand dunes, leading to different orientations for a given wind regime. These orientations are calculated from the sediment flux, the wind speed-up effect (that is, the increase in wind speed due to the convergence of the flow lines over the topography of the dune) and the aspect ratio of the dune $\frac{H}{W}$, where H is the height and W is the width of the dune. Generally, the flux-up ratio $\gamma = \beta\frac{H}{W} = 1.6$, where β is a dimensionless coefficient that accounts for the speed-up effect[25]. The saltation snow flux (Q) is calculated using the saltation flux from ref. 63 using

$$Q = \frac{\rho_{\mathrm{air}}}{g} \frac{u_{\mathrm{f}}}{u_*^{\mathrm{th}}} u_*^2 (u_* - u_*^{\mathrm{th}}), \tag{2}$$

where ρ_{air} is the air density, g is the gravitational acceleration, u_{f} is the particle fall velocity (set to 0.75 m s^{-1}, as in ref. 63), u_* is the friction velocity and u_*^{th} is the threshold friction velocity for transport, that is, the minimum friction velocity needed to mobilize snow from the surface and initiate transport by saltation[63]. The friction velocity is given by $u = \frac{u_*}{\kappa}\ln\left(\frac{z}{z_0}\right)$, where z_0 is the aerodynamic roughness length (which is set to 1 mm), $\kappa = 0.4$ is the Von Kàrmàn constant and u is the wind speed at the height $z = 10$ m given by the ERA5 reanalysis. The threshold wind speed for snow transport depends on the surface snow properties[64,65], which are not sufficiently well constrained to estimate the threshold wind speed in Antarctica. Therefore, the wind threshold wind speed was set to 6 m s^{-1} on the basis of empirical observations[35]. The sensitivity to this parameter was tested, and the mean difference of direction for the flux with a threshold wind speed at 8 m s^{-1} is 5°, and the RMSE is 10°. It is worth noting that this threshold wind speed is different from the threshold wind speed for maintaining the saturated snow flux. It is generally lower than the threshold wind speed required to remobilize snow from the surface[44].

From the snow flux, the elongating and bed-instability mode orientations can be calculated. The elongating mode orientation $\alpha_{\mathrm{elongation}}$ is given by

$$\tan\alpha_{\mathrm{elongation}} = \frac{<\overrightarrow{Q(\alpha_{\mathrm{elongation}})}> \cdot \vec{j}}{<\overrightarrow{Q(\alpha_{\mathrm{elongation}})}> \cdot \vec{i}}, \tag{3}$$

where $<\overrightarrow{Q(\alpha)}>$ is the snow flux integrated over time in the direction α and $\vec{i},\vec{j}$ basis vectors, and the elongating mode orientation $\alpha_{\mathrm{elongation}}$ corresponds to the mean snow flux direction.

In the bed-instability mode, the dune grows in the direction α_i that maximizes the growth rate σ:

$$\sigma(\alpha_i) = \max\left(Q_0 \times |\sin(\theta_{\mathrm{f}} - \alpha_i) + \gamma \times \sin(\theta_{\mathrm{f}} - \alpha_i)^2|\right), \tag{4}$$

where Q_0 is the value of the saturated snow flux and θ_{f} is the angle associated with the flux. The observed dune orientation is compared with each mode orientation and the dune type is attributed to the nearest mode if the difference does not exceed ±15°.

Method limitations

- Satellite images present striping and banding, which probably originate from a defect in the sensor calibration[51]. There is no known way to detect this or remove it, so we rely on the redundancy of acquisitions to discard them.
- The spatial resolution of the satellite imagery used, at best 10 m, and the size of the subimages (2–3 km) limits the detection to dunes that are hectometres to kilometres long. The study is only about these dunes, and excludes the megadunes, the sastrugi (metre-scale erosional bedforms) and other smaller bedforms (barchans, ripples and so on). It is worth mentioning that sastrugi usually coexist with long dunes, and they have a different orientation (for example, Fig. 1g and Supplementary Fig. 13). Many open questions remain about these dunes. Their size, dynamics and even orientation are not properly understood. Sastrugi are reported to be scoured by katabatic winds and to align in their direction[3], which is consistent with our observations on the Pléaides image (Fig. 1g and Supplementary Fig. 13). However, no global study has yet demonstrated this.
- The resolution of the wind data (0.25° × 0.25°, corresponding to approximately 55 km × 5 km in some regions and 55 km × 55 km in others, depending on the area's latitude) is adequate for continent-wide analysis but is too coarse for a detailed interpretation of our data at 2.5 km resolution. The high resolution of our dataset is not fully exploited in this study.
- The study is limited to summer time, owing to the use of optical imagery, and uses 4 years of data. The study focuses on the continental pattern over this period, and excludes more rapid dynamics of dunes as well as potential decennial changes.

Data availability

The ERA5 reanalysis hourly data on single levels from 1940 to the present are available from the Copernicus Climate Data Store at https://cds.climate.copernicus.eu/cdsapp#!/dataset/reanalysis-era5-single-levels?tab=overview. The Sentinel-2 data are available from the Copernicus Data Space Ecosystem repository at https://dataspace.copernicus.eu/. The Landsat 8 data are available from the US Geological Survey online repository at https://earthexplorer.usgs.gov/. The datasets generated during the current study are available from the Earth System Data Repository at https://doi.org/10.57932/720db223-3073-465b-a427-d5742235dcfe.

References

51. *Landsat 8 (L8) Data Users Handbook* No. LSDS-1574, Version 5.0 (US Geological Survey, 2019).
52. *Sentinel-2 User Handbook* (European Space Agency, 2015).
53. Mouginot, J., Scheuchl, B. & Rignot, E. Mapping of ice motion in Antarctica using synthetic-aperture radar data. *Remote Sens.* **4**, 2753–2767 (2012).
54. Rignot, E., Mouginot, J. & Scheuchl, B. Ice flow of the Antarctic ice sheet. *Science* **333**, 1427–1430 (2011).
55. Hui, F. et al. Mapping blue-ice areas in Antarctica using ETM+ and MODIS data. *Ann. Glaciol.* **55**, 129–137 (2014).
56. Matsuoka, K., Skoglund, A. & Roth, G. *Quantarctica (dataset)* (Norwegian Polar Institute, 2018); https://doi.org/10.21334/npolar.2018.8516e961
57. Moussavi, M., Pope, A., Halberstadt, A. R. W. & Abdalati, W. Antarctic supraglacial lake detection using Landsat 8 and Sentinel-2 imagery: towards continental generation of lake volumes. *Remote Sens.* **12**, 134 (2020).
58. Taylor, C. C. Automatic bandwidth selection for circular density estimation. *Comput. Stat. Data Anal.* **52**, 3493–3500 (2008).
59. Hersbach, H. et al. The ERA5 global reanalysis. *Q. J. R. Meteorol. Soc.* **146**, 1999–2049 (2020).
60. Caton Harrison, T. et al. Reanalysis representation of low-level winds in the Antarctic near-coastal region. *Weather Clim. Dyn.* **3**, 1415–1437 (2022).
61. Tetzner, D., Thomas, E. & Allen, C. A validation of ERA5 reanalysis data in the southern Antarctic Peninsula—Ellsworth Land region, and its implications for ice core studies. *Geosciences* **9**, 289 (2019).
62. Gossart, A. et al. An evaluation of surface climatology in state-of-the-art reanalyses over the Antarctic Ice Sheet. *J. Clim.* **32**, 6899–6915 (2019).
63. Schmidt, R. A. Properties of blowing snow. *Rev. Geophys.* **20**, 39–44 (1982).
64. He, S. & Ohara, N. A new formula for estimating the threshold wind speed for snow movement. *J. Adv. Model. Earth Syst.* **9**, 2514–2525 (2017).
65. Li, L. & Pomeroy, J. W. Estimates of threshold wind speeds for snow transport using meteorological data. *Am. Meteorol. Soc.* **36**, 205–213 (1997).
66. Crameri, F. Scientific colour maps. *Zenodo* https://zenodo.org/records/4491293 (2021).

Acknowledgements

M.P. acknowledges ENS Paris-Saclay for funding. C.N. acknowledges the financial support of the French National Research Agency through grants ANR-18-IDEX-0001 and ANR-23-CE56-0008. Perceptually uniform colour maps are used in certain figures[66]. We acknowledge the Norwegian Polar Institute's Quantarctica package[56].

Author contributions

With advice from L.A., G.P. and C.N., M.P. processed the Sentinel-2 and Landsat 8 images. C.N. facilitated the analysis and comparison of the results with the sand dune theory. C.A. aided in interpreting the results. F.B. processed the Pléiades image. M.P. wrote the paper with input from all authors.

Competing interests

The authors declare no competing interests.

Additional information

Extended data is available for this paper at https://doi.org/10.1038/s41561-024-01506-1.

Supplementary information The online version contains supplementary material available at https://doi.org/10.1038/s41561-024-01506-1.

Correspondence and requests for materials should be addressed to Ghislain Picard.

Peer review information *Nature Geoscience* thanks Simon Filhol and Giacomo Traversa for their contribution to the peer review of this work. Primary Handling Editor: Tamara Goldin, in collaboration with the *Nature Geoscience* team.

https://doi.org/10.1038/s41561-024-01506-1

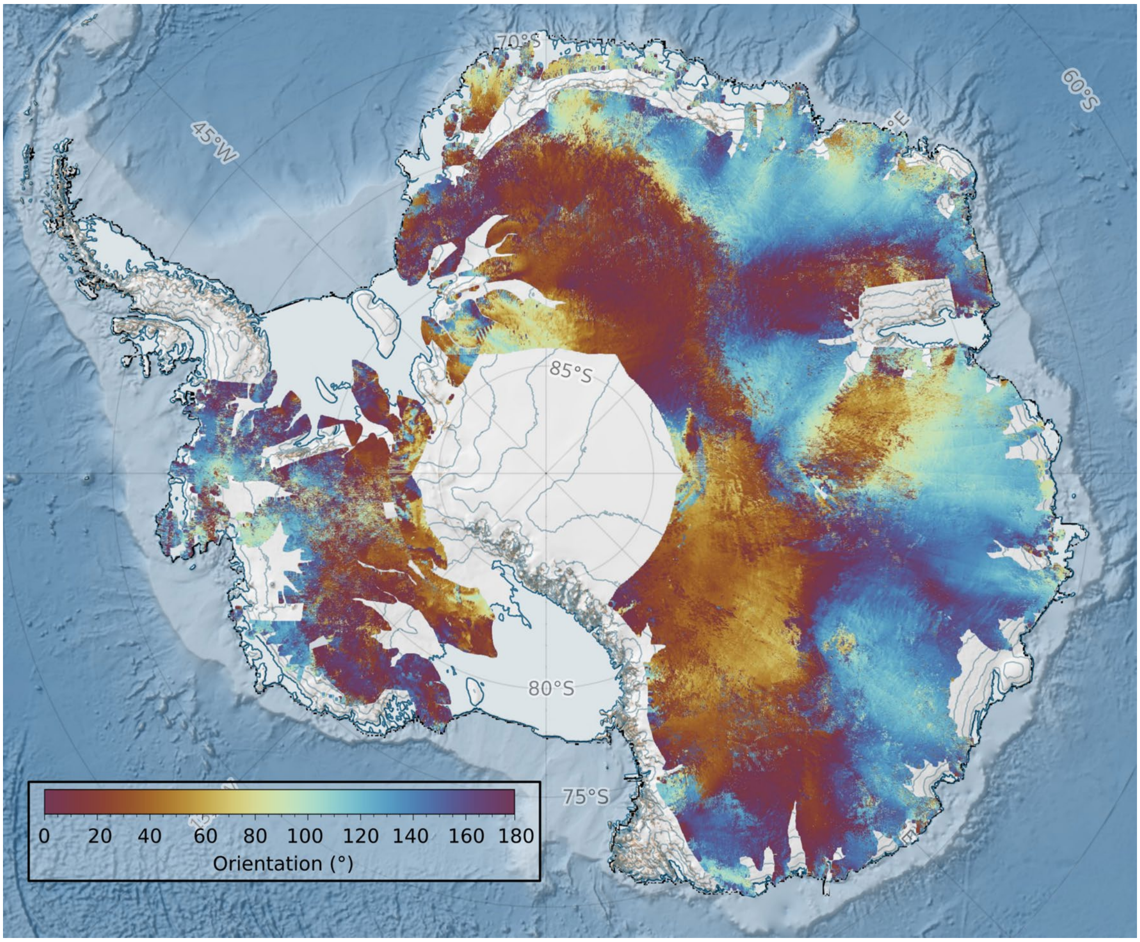

Extended Data Fig. 1 | Map of the dune orientation at high-resolution. Map of the dune orientation at 2.5 × 2.5 km^2 resolution retrieved from satellite imagery in November and December 2018–2021.